



HAL
open science

Initial stages of graphitization on SiC(000-1), as studied by phase atomic force microscopy

F.J. Ferrer, E. Moreau, D. Vignaud, D. Deresmes, S. Godey, X. Wallart

► To cite this version:

F.J. Ferrer, E. Moreau, D. Vignaud, D. Deresmes, S. Godey, et al.. Initial stages of graphitization on SiC(000-1), as studied by phase atomic force microscopy. *Journal of Applied Physics*, 2011, 109 (5), pp.054307-1-6. 10.1063/1.3560896 . hal-00577059

HAL Id: hal-00577059

<https://hal.science/hal-00577059>

Submitted on 25 May 2022

HAL is a multi-disciplinary open access archive for the deposit and dissemination of scientific research documents, whether they are published or not. The documents may come from teaching and research institutions in France or abroad, or from public or private research centers.

L'archive ouverte pluridisciplinaire **HAL**, est destinée au dépôt et à la diffusion de documents scientifiques de niveau recherche, publiés ou non, émanant des établissements d'enseignement et de recherche français ou étrangers, des laboratoires publics ou privés.

Initial stages of graphitization on SiC(000-1), as studied by phase atomic force microscopy

Cite as: J. Appl. Phys. **109**, 054307 (2011); <https://doi.org/10.1063/1.3560896>

Submitted: 02 December 2010 • Accepted: 31 January 2011 • Published Online: 10 March 2011

F. J. Ferrer, E. Moreau, D. Vignaud, et al.



View Online



Export Citation

ARTICLES YOU MAY BE INTERESTED IN

[Hydrogen intercalation of epitaxial graphene and buffer layer probed by mid-infrared absorption and Raman spectroscopy](#)

AIP Advances **8**, 045015 (2018); <https://doi.org/10.1063/1.5024132>

[The quasi-free-standing nature of graphene on H-saturated SiC\(0001\)](#)

Applied Physics Letters **99**, 122106 (2011); <https://doi.org/10.1063/1.3643034>

[Influence of the silicon carbide surface morphology on the epitaxial graphene formation](#)

Applied Physics Letters **99**, 111901 (2011); <https://doi.org/10.1063/1.3638058>

Lock-in Amplifiers
up to 600 MHz



Zurich
Instruments



Initial stages of graphitization on SiC(000-1), as studied by phase atomic force microscopy

F. J. Ferrer,^{a)} E. Moreau, D. Vignaud,^{b)} D. Deresmes, S. Godey, and X. Wallart
*Institut d'Electronique, de Microélectronique et de Nanotechnologie (IEMN, UMR CNRS 8520), Av. Poincaré,
 PO Box 60069, 59652 Villeneuve d'Ascq Cedex, France*

(Received 2 December 2010; accepted 31 January 2011; published online 10 March 2011)

The initial stages of graphitization on 4H- and 6H-SiC (000-1) under ultrahigh vacuum at temperatures of 1125–1175°C have been studied by atomic force microscopy (AFM), X-ray photoemission spectroscopy and reflected high energy electron diffraction. A progressive coverage of the surface by graphene has been observed depending on the time and temperature of annealing. Graphene growth mainly starts from the step edges, although it sometimes nucleates in the middle of a SiC terrace. Comparison of the topographic and phase AFM images shows that the latter are the most efficient for identifying graphene before complete coverage of the surface. © 2011 American Institute of Physics. [doi:10.1063/1.3560896]

I. INTRODUCTION

Graphene, a single layer of carbon where the sp² bonding configuration forms a hexagonal lattice, has attracted the attention of researchers in recent years. Its exciting electronic properties include massless Dirac fermions and the room temperature quantum Hall effect.^{1–3} The very high mobility and the possibility to tune the electronic conduction via field effect^{4–6} make graphene a very promising material for future microelectronic applications. In the nonelectronic field, one example of application among others is the ability to detect single gas molecules adsorbed on its surface.⁷

Up to now, graphene has been obtained mainly by three different ways. The first method consists of exfoliating graphene layers from bulk graphite and transferring them onto oxidized silicon.⁸ The second one, the so-called graphitization process, involves heating bulk silicon carbide to induce Si preferential sublimation, resulting in epitaxial graphene growth on the SiC surface.^{9,10} The chemical vapor deposition constitutes the third method and relies on growth from hydrocarbon gases on metallic substrates (for example on Ni¹¹). Some other processes have also shown their ability to grow graphene layers, like plasma assisted deposition,¹² reduction of graphite oxide,¹³ and molecular beam epitaxy.¹⁴ From the three more mature techniques mentioned before, graphitization appears to be the most compatible with usual planar processing for electronic applications without any delicate transfer of the graphene films.

Hexagonal SiC crystals have a polar *c* axis, which means the two opposite faces of the SiC along this axis terminate with different atoms, i.e. silicon atoms on the Si-face (0001) or carbon atoms on the other (000-1). An understanding of the thermodynamics and kinetics of graphene formation at the surface of SiC is still lacking. The graphitization-induced graphene characteristics (growth rate, structure, etc.) are strongly face-dependent.¹⁵ Only a few studies have been

devoted to the initial stage of graphene growth, mainly on the Si-face of SiC.^{16–19} Despite the fact that the C face leads to higher electron mobilities,^{20–22} a similar knowledge of graphitization on this face has not yet been reached.^{23–26} Two techniques have been used for graphitization on the C-face of SiC. One involves ultrahigh vacuum (UHV) experiments at temperatures above 1100 °C, while the other implies low-vacuum enclosed furnaces at significantly higher temperatures (minimum of 1420 °C).¹⁵ The latter one leads to the best material in terms of domain size and mobility. But, probably because of a poor control of low-thickness graphene growth, high-frequency nanodevices using such high mobility low-vacuum graphene have not been published so far. Indeed, the best graphene high-frequency nanodevices, which require thin layers for efficient field effect modulation, have been achieved with UHV material grown on the Si face.^{27,28} A better knowledge of the growth mechanisms at the onset of graphitization on (000-1) SiC is thus required. Since this implies a good control of the growth at low thickness, we have focused our study on the first steps of UHV graphitization on SiC (000-1).

II. EXPERIMENTAL DETAILS

We used 6H- and 4H-SiC (000-1) substrates nominally on-axis (miscut angle lower than 0.5°) purchased from Cree and SiCrystal and chemo-mechanically polished by Novasic. Substrate preparation and flattening was carried out under a long Si flux exposure at 1100°C as described in a previous article,²⁹ leading to a step-terrace structure with half-period step height and a root-mean-square (rms) roughness in the range 0.05–0.07 nm for 1 μm² single-terrace surface. Samples were then annealed in the 1125–1175 °C temperature range, for less than one minute up to 30 mins, in an ultrahigh vacuum (UHV) chamber (base pressure in the low 10⁻¹⁰ Torr). Each sample was used for only one growth test, without any attempt of regrowth. Real-time surface crystallography was characterized by reflection high-energy electron diffraction (RHEED) operating at 15 kV. The sample temperature was

^{a)}Present address: Centro Nacional de Aceleradores, U. Sevilla- CSIC, Av. Thomas A. Edison 7, E-41092 Sevilla, Spain. Electronic mail: fjferrer@us.es.

^{b)}Electronic mail: dominique.vignaud@univ-lille1.fr.

measured using an optical pyrometer with an effective emissivity set to 0.35. Topographic and phase atomic force microscopy (AFM) observations were achieved in air by tapping mode, using Multimode or Picoforce Veeco equipments with a Nanoscope IVa controller. The WSxM4.0 software was used for AFM image processing.³⁰ The surface chemical composition was analyzed by ex situ photoelectron spectroscopy, thus requiring transfer of the samples at room pressure. Angle resolved X-ray photoelectron spectroscopy (ARXPS) experiments (at 25, 45, and 70°, measured from the sample surface) were done to obtain spectra with variable surface sensitivity, from which the thickness of the graphene layer could be evaluated.³¹

III. RESULTS

After the initial smoothening process under Si flux, the temperature was increased up to 1125–1175°C. The RHEED pattern first displays the C-rich (3×3) surface reconstruction and the higher the temperature is, the faster this reconstruction appears. Figure 1 shows topographic and phase images of a sample annealed at 1150°C during 1 minute. The initial step-terrace structure of the substrate is still observed, but the terrace surface rms roughness has slightly increased: it is now 0.08 nm (measured on a 0.5 μm² surface) compared with the initial value of 0.05–0.07 nm. In addition, a modification of the surface at the step edges is clearly observed on the topographic image (Fig. 1a), where some kind of erosion/decomposition appears to have started all along the substrate edges. Some contrast in the associated phase image (Fig. 1b) is also observed, which does not strictly correspond to the topographic one. When the samples are annealed for a longer time (10, 20 and 30 mins at 1150°C), some remnants of the step-terrace structure are still observed, as shown in the AFM topographic images Figs. 2(a), 2(d), and 2(g), but these terraces are no longer flat and steps are no longer straight. Some erosion also appears in the middle of terraces, as indicated for example by the circle in Fig. 2(a). A mean depth of 0.3–0.4 nm has been found for the pits located in the middle of the terraces. The corresponding phase images displayed in Figs. 2(b), 2(e), and 2(h) show a bimodal distribution after annealing, as seen in Figs. 2(c), 2(f), and 2(i). Since the phase image contrast originates from both the surface topography and the material hardness, this observation suggests the

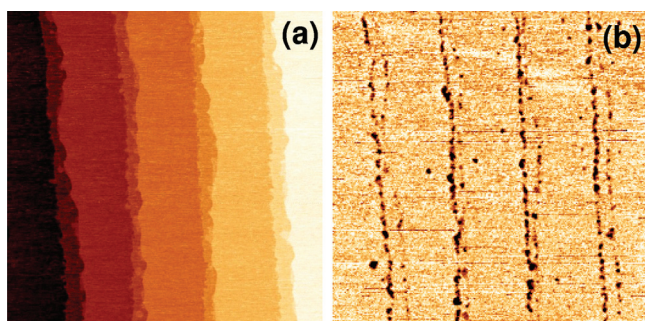


FIG. 1. (Color online) The 2×2 μm² AFM topographic (a) and phase (b) images of a 6H-SiC (000-1) substrate annealed one minute at 1150°C. Local flattening on one single terrace has been achieved in (a) to emphasize the atomically flat terrace structure. Vertical scales are 4 nm (a) and 3° (b).

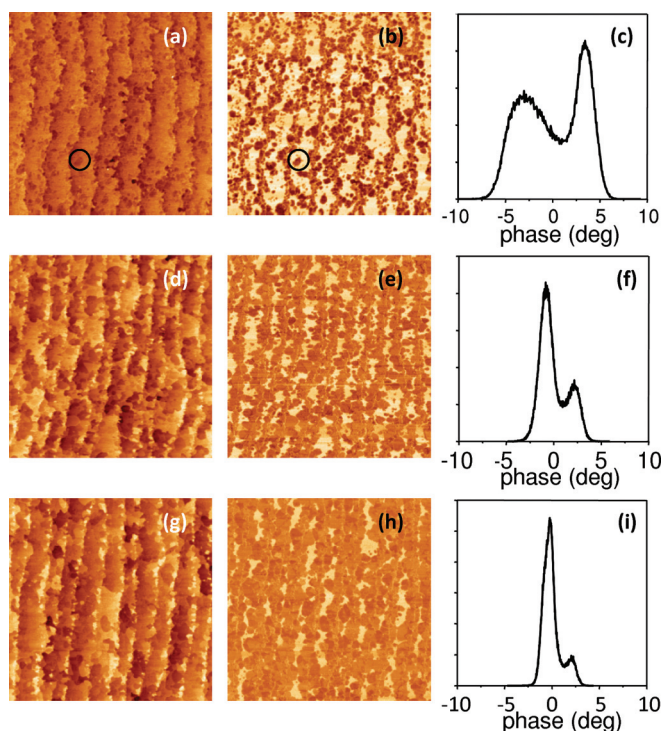


FIG. 2. (Color online) The 2×2 μm² AFM topographic (a, d, g), phase (b, e, h) images and histograms of phase values (c, f, i), of 4H-SiC (0 0 0 -1) substrates respectively annealed 10 (a, b, c), 20 (d, e, f) and 30 mins (g, h, i) at 1150°C. Vertical scales are 2 nm (a, d, g), 15° (b) and 10° (e, h).

presence of two different materials on the sample surface.¹⁸ For discussion purposes here, we refer to the percentage of area covered by this second material as the 2nd phase. At a fixed temperature, when the annealing time increases, the 2nd phase coverage also increases, as observed in Figs. 2(b), 2(e), and 2(h). It is also observed that, for an identical annealing time, a higher annealing temperature leads to a larger 2nd phase coverage. These two experimental observations are illustrated in Fig. 3, where the 2nd phase coverage is plotted versus the annealing time and temperature.

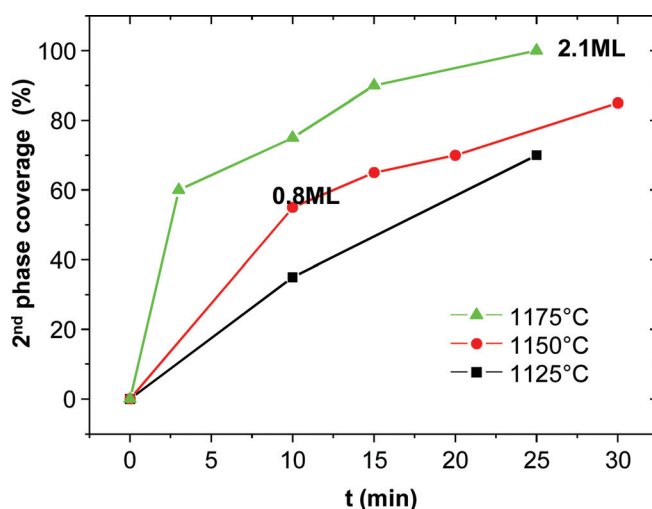


FIG. 3. (Color online) The 2nd phase coverage, from the AFM phase images, for different annealing times and temperatures. The graphene thickness deduced from XPS measurements is indicated close to the corresponding points.

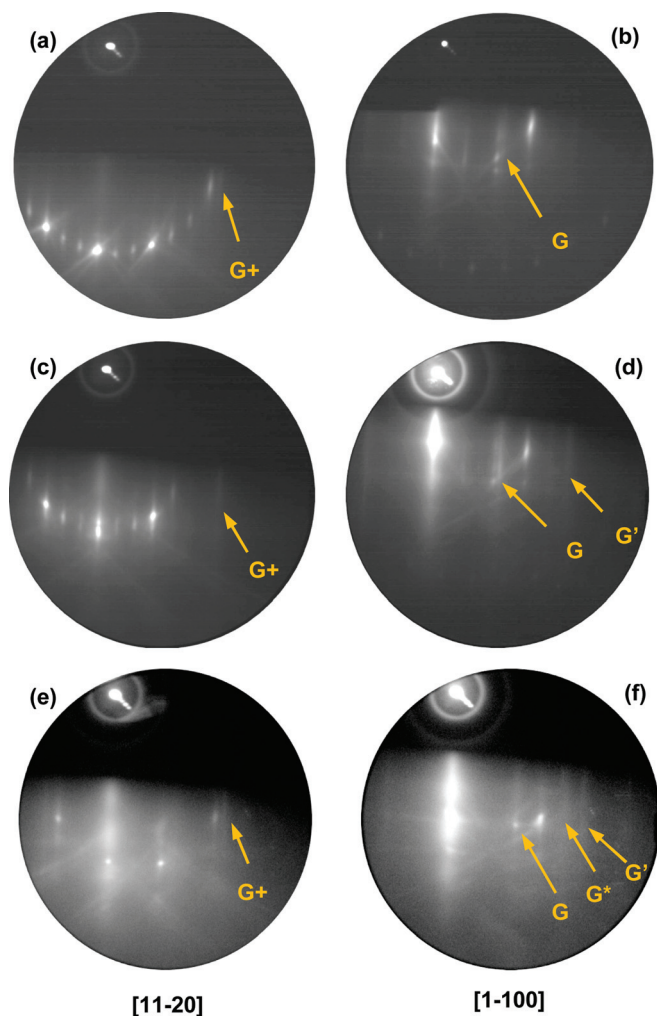


FIG. 4. (Color online) RHEED patterns along the [11-20] (a, c, e) and [1-100] (b, d, f) azimuths of 4H-SiC (000-1) substrates annealed 10 (a, b) and 30 (c, d) minutes at 1150°C, and a 6H-SiC (000-1) annealed 25 mins at 1175°C (e, f). Orange arrows show the graphene-related diffraction components.

When the 2nd phase coverage reaches 50%, a well defined (3×3) RHEED pattern is observed (Figs. 4(a) and 4(b)) as well as a very weak graphene signal (see arrows in Fig. 4). The combined SiC/(3×3)/graphene reciprocal lattice is schematized in Fig. 5 for comparison with the experimental diffraction pattern. It must be mentioned that the diffraction spot shown by the G arrow includes almost superimposed contributions from both the (3×3) reconstruction and the graphene. This is most easily seen in Fig. 4d. When the 2nd phase coverage reaches 85%, the (3×3) reconstruction is still observed together with the growing intensity graphene spots (Figs. 4(c) and 4(d)), mainly along the [1-100] direction (see the G arrow in Fig. 4d). A diffraction pattern dominated by graphene is observed when the sample is annealed 25 mins at 1175°C (Figs. 4(e), 4(f) and 5). In this last sample, the 2nd phase coverage is equal to 100% and the (3×3) reconstruction has disappeared. The LEED pattern of this latest sample, (not shown here), displays the (1×1) SiC spots together with diffuse and incomplete graphene arc segments with maxima around $\pm 10^\circ$ from the [11-20] direction.

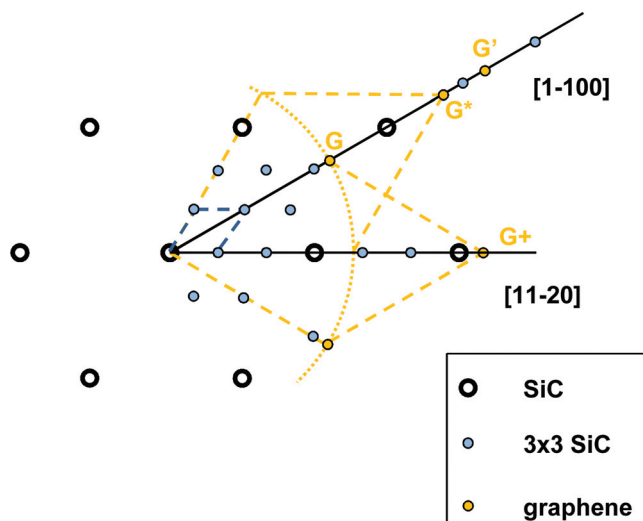


FIG. 5. (Color online) The reciprocal lattices of SiC, including the 3×3 surface reconstruction, and of continuously rotated graphene (circle arcs).

XPS spectra of three samples with different 2nd phase coverage are shown in Fig. 6. The AFM images of the 1% and 60% 2nd phase coverage samples are respectively shown in Fig. 1 and Figs. 2(a) and 2(b). The corresponding observations for the 100% 2nd phase coverage sample are not shown. Two peaks are observed for the C1s signal: the first one, at ~ 282.8 eV, corresponds to C bonds in the substrate (C-Si); the second one, which shifts from 284.8 eV down to 284.6 eV while increasing the 2nd phase coverage, is assigned to C-C bonds in the graphene layer. Both energy positions correspond to those reported in the literature for these components on the C-face surface.^{32,33} Spectra were normalized in Fig. 6 in order to compare their relative contribution. The higher the 2nd phase coverage, the more the C-C contribution appears in the spectra. The angle-dependent C-Si bulk component attenuation allows calculating the thickness of a homogeneous layer of graphene over the SiC substrate. This procedure does not work for the 1% 2nd phase coverage sample, for which the C-Si bulk attenuation is not accurately measurable.

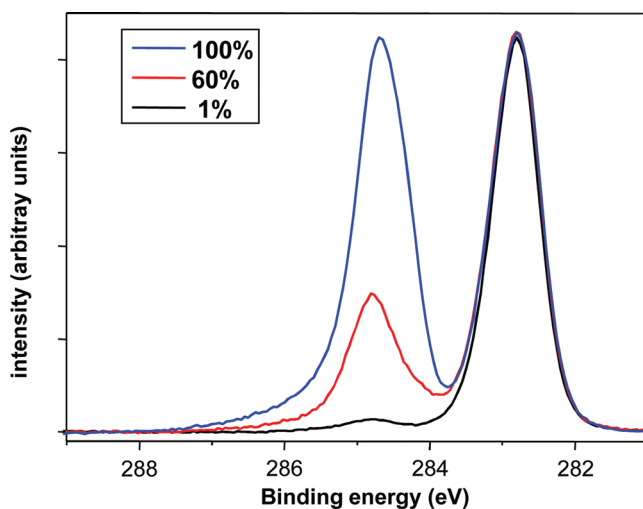


FIG. 6. (Color online) Normalized XPS spectra of SiC (000-1) samples, for different 2nd phase coverage in the AFM phase images. C-Si bulk (282.8 eV) and C-C (284.6-284.8 eV) components are observed.

ARXPS of a sample that is not completely covered by the second material (10 mins at 1150 °C; 60% 2nd phase coverage) leads to a thickness of 0.8 monolayer (ML) of graphene. This 0.8 ML value is equivalent to a graphene coverage of 80%, assuming that single layer graphene is only present. For the sample showing a complete 2nd phase coverage (25 mins at 1175 °C), the graphene thickness obtained was 2.1 ML. The ARXPS-calculated thicknesses do not depend on the chosen model for describing the graphene topography, either continuous³¹ or discrete.³⁴

IV. DISCUSSION

Since the AFM phase is sensitive to material mechanical properties,³⁵ the observed bimodal phase distribution suggests that two different materials are present on the surface after annealing. Some authors found a correlation between the phase change on AFM images and the onset of graphitization complementing the first information by STM,¹⁸ LEEM¹⁶ and Raman.³⁶ For the Si-face, Bolen *et al.*¹⁸ obtained a clear AFM phase contrast between 1 nm deep pits with a graphene-covered bottom and graphene-free 0.5 nm shallower pits (probably corresponding to the $(6\sqrt{3}\times 6\sqrt{3})R30^\circ$ surface reconstruction). These results suggest that only graphene is responsible for an AFM phase contrast, while C-rich reconstructions without graphene do not. This point is consistent with the AFM data of the 1% 2nd phase coverage sample (see Fig. 1), for which a strong (3×3) surface reconstruction has been observed by electron diffraction, whereas no graphene could be detected. The corresponding phase contrast (Fig. 1(b)) can be explained by the sample topography alone.

In this study, we observed that the occurrence of a phase contrast in AFM experiments is correlated with a surface C enrichment, as shown by ARXPS measurements, and with the appearance of graphene diffraction spots, as seen on the RHEED/LEED patterns. We have also shown that the graphene thickness and 2nd phase coverage are quantitatively correlated. Indeed, there are discrepancies (60% coverage-0.8 ML and 100%-2.1 ML) between AFM and ARXPS measurements, but these could be due to those two techniques not measuring precisely the same quantity. The AFM 2nd phase coverage is related to the graphene-covered surface, whatever its thickness, while the ARXPS experiments measure the total graphene volume. This discrepancy (60% coverage for 0.8 ML) suggests that some parts are already covered with a graphene bilayer before completion of the first graphene layer on the whole surface. We checked that the ARXPS-calculated graphene thickness does not depend on the continuous or discrete topographical model for the graphene layer. Since the C-rich (3×3) reconstruction leads to a C1s XPS component very close to the C1s graphene one,^{32,33} it can contribute to the ARXPS C-C peak, leading to an overestimated graphene thickness. This reconstruction may be located either between graphene regions or even under graphene. Hiebel *et al.*²⁶ already observed graphene over (3×3) or (2×2) reconstructions using STM at the onset of graphitization on the C-face. Finally, because of the atmospheric pressure transfer, oxidized bonds C-O may also contribute to the C-C component ($E_{C-O}-E_{C1s} = 1.5$ eV³⁷).

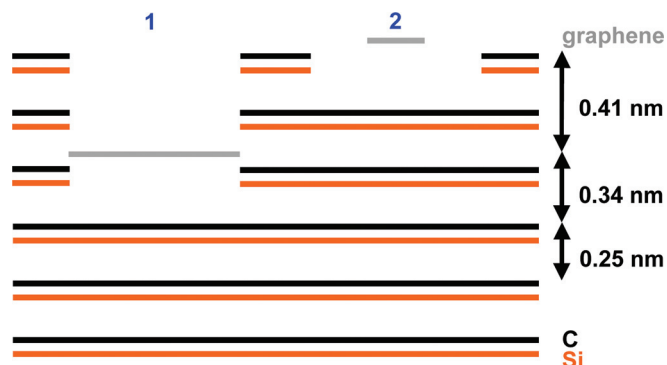


FIG. 7. (Color online) Stacking of SiC bilayers along the $\langle 0001 \rangle$ direction and graphitization topographical scheme, showing the deep pit with a graphene bottom model (1) and the partially graphitized surface model (2).

However, since the discrepancy for an incomplete coverage (60% coverage and 0.8 ML graphene) remains small, we consider graphene to be mainly responsible for the AFM phase contrast.

The AFM topographic and phase images do not strictly correspond each other (see for example the center area in Figs. 2(g) and 2(h); numerous other areas might be found on Figs. 2(d) and 2(e)). This observation has implications about the graphitization mechanisms. Whatever the SiC polytype, $\{0001\}$ SiC is made of a stack of SiC bilayers (see scheme Fig. 7). It is well known that atomic conservation implies that the C atoms from ~ 3 SiC bilayers are required to form one single graphene layer.¹⁵ These C atoms may come either from stacked SiC bilayers, resulting in graphene layers at the bottom of pits surrounded by SiC bare surface (see model 1 in Fig. 7), or from one single SiC surface bilayer, resulting in one third of the surface being covered by graphene above the SiC substrate (see model 2 in Fig. 7). Both models lead to different step heights on the surface, which are 0.41 nm for the 1st one and 0.09, 0.25, or 0.34 nm for the 2nd. The problem becomes even more tricky if one takes into account the SiC substrate step height, 0.5 nm for the 4H polytype and 0.75 nm for 6H-SiC. The topographic and phase images should be almost identical in the 1st model, because of the full coverage of the pit with graphene. On the contrary, they may differ in the 2nd, because of the simultaneous observation of very close 0.25 and 0.34 nm step heights corresponding to different set of materials (SiC/SiC for 0.25 nm without phase contrast, SiC/graphene for 0.34 nm with phase contrast). The lack of strict coincidence between the experimental AFM topographic and phase images and the complicated surface topography suggests that the 2nd model mostly applies for UHV graphitization from the step edges in the 1125–1175 °C temperature range. On the contrary, the 1st model seems consistent with the graphitization observed in the middle of terraces (see Figs. 2(a) and 2(b)), with an experimental depth of 0.3–0.4 nm to be compared to the expected 0.41 nm value.

From this point we can observe how nucleation of graphene begins at the step edges, a mechanism which has been already proposed by other authors for graphitization over the Si-face.^{38–41} Similar structures of graphene nucleation parallel to the step edges have been obtained by Raman spectroscopy³⁶

or low energy electron microscopy (LEEM) measurements.^{16,19} The C-face study of Hiebel *et al.*²⁶ for samples annealed at 1175 °C for 15 mins under UHV conditions does not show images at a scale large enough to see this kind of structure, but areas covered either with a graphene monolayer or with the (3×3) reconstruction were simultaneously observed on STM images. The same incomplete graphitization and coexistence with (3×3) reconstruction should also apply for our samples because the preparation conditions were similar.

On the Si face, Robinson³⁶ associated the nucleation of graphene from the steps with the higher density of dangling bonds in these steps with respect to the one of the terraces. Even if we are working with the opposite face of SiC, this argument still applies. Graphitization should mainly start from the edges, although a limited number of graphitized zones have been observed in the middle of the terraces. Next, C mobility could produce the expansion of graphene to both sides of the edges until the total coverage of the surface is obtained. During this lateral growth, Si sublimation produces the change of the substrate topography that degrades the initial step-terrace structure. Our AFM observations, which show graphene nucleation from the step edges, are consistent with previous studies,²⁵ but clearly differ from the ones by Camara *et al.*²³ These authors have concluded that graphene is mainly nucleated at defects, such as dislocations. The most obvious difference between these experiments seems to be the graphitization temperature and pressure range, although the substrate initial surface and preparation procedures might be important also. Graphitization is observed at temperatures as low as 1120 °C under UHV conditions,²⁵ while no graphene could be detected below 1500 °C at 10⁻⁶ Torr pressure. One may speculate that these differences come from temperature-dependent efficient Si sublimation channels, but further work is required to fully understand this effect. It is also clear that, because of the large difference in graphitization temperatures, the growth mechanisms which are discussed here for UHV graphene experiments may not directly apply to the low-vacuum case.¹⁵

Let us finally mention that the SiC (3×3) reconstruction has been systematically obtained for an annealing temperature in the 1125–1175 °C range, before the onset of graphitization, as was already observed by others^{26,32,33,42–47} for similar temperatures. At this point, we can only state that the (3×3) reconstruction is a mandatory step toward the formation of graphene on SiC C-face.

V. CONCLUSIONS

The initial growth by Si sublimation of graphene layers at 1125–1175 °C under UHV conditions was studied on SiC (000-1) substrates. Nucleation of graphene was observed at the step edges, followed by a progressive expansion until the total coverage of the surface is produced. This expansion is faster for higher temperatures and produces hard changes in the original substrate step-terrace structure.

ACKNOWLEDGMENTS

This work was achieved with the financial support of the European Union (FEDER), the ANR (project Xp-Graphene), and the Nord-Pas de Calais Regional Council.

- ¹K. S. Novoselov, A. K. Geim, S. V. Morozov, D. Jiang, M. I. Katsnelson, I. V. Grigorieva, S. V. Dubonos, A. A. Firsov, *Nature* **438**, 197 (2005).
- ²Y. Zhang, Y.-W. Tan, H. L. Stormer, and P. Kim, *Nature* **438**, 201 (2005).
- ³K. S. Novoselov, Z. Jiang, Y. Zhang, S. V. Morozov, H. L. Stormer, U. Zeitler, J. C. Maan, G. S. Boebinger, P. Kim, and A. K. Geim, *Science* **315**, 1379 (2007).
- ⁴J. Hass, R. Feng, T. Li, X. Li, Z. Song, W. A. de Heer, P. N. First, E. H. Conrad, C. A. Jeffrey, and C. Berger, *Appl. Phys. Lett.* **89**, 143106 (2006).
- ⁵D. A. Areshkin, D. Gunlycke, and C. T. White, *Nano Lett.* **7**, 204 (2007).
- ⁶S. Watcharotone, D. A. Dikin, S. Stankovich, R. Piner, I. Jung, G. H. B. Dommett, G. Evmenenko, S.-E. Wu, S.-F. Chen, C.-P. Liu, S. T. Nguyen, R. S. Ruoff, *Nano Lett.* **7**, 1888 (2007).
- ⁷F. Schedin, A. K. Geim, S. V. Morozov, E. W. Hill, P. Blake, M. I. Katsnelson, and K. S. Novoselov, *Nat. Mater.* **6**, 652 (2007).
- ⁸K. S. Novoselov, A. K. Geim, S. V. Morozov, D. Jiang, Y. Zhang, S. V. Dubonos, I. V. Grigorieva, and A. A. Firsov, *Science* **306**, 666 (2004).
- ⁹A. J. Van Bommel, J. E. Crombeen, and A. Van Tooren, *Surf. Sci.* **48**, 463 (1975).
- ¹⁰E. Rollings, G.-H. Gweon, S. Y. Zhou, B. S. Mun, J. L. McChesney, B. S. Hussain, A. V. Fedorov, P. N. First, W. A. de Heer, and A. Lanzara, *J. Phys. Chem. Sol.* **67**, 2172 (2006).
- ¹¹K. S. Kim, Y. Zhao, H. Jang, S. Y. Lee, J. M. Kim, K. S. Kim, J.-H. Ahn, P. Kim, J.-Y. Choi, and B. H. Hong, *Nature* **457**, 706 (2009).
- ¹²A. Malesevic, R. Vitchev, K. Schouteden, A. Volodin, L. Zhang, G. Van Tendeloo, A. Vanhulsel, and C. Van Haesendonck, *Nanotechnology* **19**, 305604 (2008).
- ¹³S. Stankovich, D. A. Dikin, R. D. Piner, K. A. Kohlhaas, A. Kleinhammes, Y. Jia, Y. Wu, S. T. Nguyen, and R. S. Ruoff, *Carbon* **45**, 1558 (2007).
- ¹⁴E. Moreau, F. J. Ferrer, D. Vignaud, S. Godey, X. Wallart, *Phys. Status Solidi A* **207**, 300 (2010).
- ¹⁵J. Hass, W. A. de Heer, and E. H. Conrad, *J. Phys. Condens. Matter* **20**, 323202 (2008).
- ¹⁶J. B. Hannon and R. M. Tromp, *Phys. Rev. B* **77**, 241404 (2008).
- ¹⁷C. Riedl, U. Starke, J. Bernhardt, M. Franke, and K. Heinz, *Phys. Rev. B* **76**, 245406 (2007).
- ¹⁸M. L. Bolen, S. E. Harrison, L. B. Biedermann, and M. A. Capano, *Phys. Rev. B* **80**, 115433 (2009).
- ¹⁹T. Ohta, N. C. Bartelt, S. Nie, K. Thürmer, and G. L. Kellogg, *Phys. Rev. B* **81**, 121411R (2010).
- ²⁰J. H. Chen, C. Jang, S. Xiao, M. Ishigami, and M. S. Fuhrer, *Nat. Nanotechnol.* **3**, 206 (2008).
- ²¹K. I. Bolotin, K. J. Sikes, J. Hone, H. L. Stormer, and P. Kim, *Phys. Rev. Lett.* **101**, 096802 (2008).
- ²²J. L. Tedesco, B. L. VanMil, R. L. Myers-Ward, J. M. McCrate, S. A. Kitt, P. M. Campbell, G. G. Jernigan, J. C. Culbertson, C. R. Eddy, Jr., and D. K. Gaskill, *Appl. Phys. Lett.* **95**, 122102 (2009).
- ²³N. Camara, G. Rius, J. R. Huntzinger, A. Tiberj, L. Magaud, N. Mestres, P. Godignon, and J. Camassel, *Appl. Phys. Lett.* **93**, 263102 (2008).
- ²⁴N. Camara, J. R. Huntzinger, G. Rius, A. Tiberj, N. Mestres, F. Pérez-Murano, P. Godignon, and J. Camassel, *Phys. Rev. B* **80**, 125410 (2009).
- ²⁵P. Luxmi, J. Fisher, N. Srivastava, R. M. Feenstra, Y. Sun, J. Kedzierski, P. Healey, and G. Gu, *Appl. Phys. Lett.* **95**, 073101 (2009).
- ²⁶F. Hiebel, P. Mallet, F. Varchon, L. Magaud, and J.-Y. Veuillen, *Phys. Rev. B* **78**, 153412 (2008).
- ²⁷Y.-M. Lin, C. Dimitrakopoulos, K. A. Jenkins, D. B. Farmer, H.-Y. Chiu, A. Grill, and P. Avouris, *Science* **327**, 662 (2010).
- ²⁸N. Meng, F. J. Ferrer, D. Vignaud, G. Dambrine, and H. Happy, *Int. J. Microwave Wireless Technol.* **2**, 441 (2010).
- ²⁹F. J. Ferrer, E. Moreau, D. Vignaud, S. Godey, and X. Wallart, *Semicond. Sci. Technol.* **24**, 125014 (2009).
- ³⁰I. Horcas, R. Fernandez, J. M. Gomez-Rodriguez, J. Colchero, J. Gomez-Herrero, A. M. Baro, *Rev. Sci. Instrum.* **78**, 013705 (2007).
- ³¹C. S. Fadley, *Basic Concepts of X-ray Photoelectron Spectroscopy*, Vol. 2, Electron Spectroscopy: Theory, Techniques, and Applications (Academic Press, New York, 1978).
- ³²L. I. Johansson, P.-A. Glans, and N. Hellgren, *Surf. Sci.* **405**, 288 (1998).
- ³³K. V. Emtsev, F. Speck, T. Seyller, L. Ley, *Phys. Rev. B* **77**, 155303 (2008).
- ³⁴D. Y. Petrovykh, J. M. Sullivan, and L. J. Whitman, *Surf. Interface Anal.* **37**, 989 (2005).
- ³⁵J. C. Byers, P. Tamiasso-Martinon, C. Deslouis, A. Pailleret, and O. A. Semenikhin, *J. Phys. Chem. C* **114**, 18474 (2010).
- ³⁶J. Robinson, X. Weng, K. Trumbull, R. Cavaleiro, M. Wetherington, E. Frantz, M. LaBella, Z. Hughes, M. Fanton, and D. Snyder, *ACS Nano* **4**, 153 (2010).

- ³⁷C. Virojanadara and L. I. Johansson, *Surf. Sci.* **505**, 358 (2002).
- ³⁸K. V. Emtsev, A. Bostwick, K. Horn, J. Jobst, G. L. Kellogg, L. Ley, J. L. McChesney, T. Ohta, S. A. Reshanov, J. Röhl, E. Rotenberg, A. K. Schmid, D. Waldmann, H. B. Weber, and T. Seyller, *Nat. Mater.* **8**, 203 (2009).
- ³⁹M. Hupalo, E. H. Conrad, and M. C. Tringides, *Phys. Rev. B.* **80**, 041401 (2009).
- ⁴⁰S. W. Poon, W. Chen, E. S. Tok, and A. T. S. Wee, *Appl. Phys. Lett.* **92**, 104102 (2008).
- ⁴¹C. Virojanadara, R. Yakimova, J. R. Osiecki, M. Syväjärvi, R. I. G. Uhrberg, L. I. Johansson, and A. A. Zakharov, *Surf. Sci.* **603**, L87 (2009).
- ⁴²J. Bernhardt, M. Nerding, U. Starke, and K. Heinz, *J. Mater. Sci. Eng. B.* **61-62**, 207 (1999).
- ⁴³I. Forbeaux, J.-M. Themlin, and J.-M. Debever, *Surf. Sci.* **442**, 9 (1999).
- ⁴⁴A. Seubert, J. Bernhardt, M. Nerding, U. Starke, and K. Heinz, *Surf. Sci.* **454-456**, 45 (2000).
- ⁴⁵F. Takeuchi, R. Fukuyama, Y. Hoshino, T. Nishimura, and Y. Kido, *Surf. Sci.* **601**, 2203 (2007).
- ⁴⁶F. Varchon, P. Mallet, L. Magaud, and J. Y. Veullen, *Phys. Rev. B.* **77**, 165415 (2008).
- ⁴⁷U. Starke and C. Riedl, *J. Phys. Condens. Matter* **21**, 134016 (2009).